Exploiting the therapeutic vulnerability of IDH-mutant gliomas with zotiraciclib

Ying Pang[1], Guangyang Yu[1], Zach Sergi[1], Qi Li[1], Xueyu Sang[1], Olga Kim[1], Herui Wang[1], Alice Ranjan[1], Mythili Merchant[1], Belene Oudit[1], Robert W. Robey[2], Ferri Soheilian[3], Bao Tran[4], Felipe J. Núñez[5], Meili Zhang[1], Hua Song[1], Wei Zhang[1], Dionne Davis[1], Mark R. Gilbert[1], Michael M. Gottesman[2], Zhenggang Liu[6], Javed Khan[7], Craig J. Thomas[8], Maria G. Castro[5], Jing Wu[1*]

[1] Neuro-Oncology Branch, Center for Cancer Research, National Cancer Institute, National Institutes of Health, Bethesda, MD 20892, USA
[2] Laboratory of Cell Biology, National Cancer Institute, National Institutes of Health, Bethesda, MD 20892, USA
[3] Electron Microscopy Laboratory, Center for Cancer Research, National Cancer Institute, National Institutes of Health, Frederick, MD 21701, USA
[4] Frederick National Laboratory for Cancer Research, Leidos Biomedical Research, Inc., Frederick, MD 20701, USA
[5] Departments of Neurosurgery and Cell and Developmental Biology, University of Michigan Medical School, Ann Arbor, MI 48109, USA
[6] Laboratory of Immune Cell Biology, Center for Cancer Research, National Cancer Institute, National Institutes of Health, Bethesda, MD 20892, USA
[7] Oncogenomics Section, Genetics Branch, Center for Cancer Research, National Cancer Institute, NIH, Bethesda, MD 20892, USA
[8] Division of Pre-Clinical Innovation, National Center for Advancing Translational Sciences (NCATS), National Institutes of Health, Rockville, MD 20850, USA

Running title: IDH-mutant gliomas vulnerability with zotiraciclib

***Corresponding Author:** Jing Wu, MD, PhD, Neuro-oncology Branch, Center for Cancer Research, NCI, Building 37, Room 1142A, Bethesda, MD 20892. Phone: 240-760-6036; E-mail: jing.wu3@nih.gov

Abstract

Background: Isocitrate dehydrogenase (IDH)-mutant gliomas exhibit unique metabolic and biological features that may make them vulnerable to specific treatment. In this study, we investigated the selective vulnerability of IDH-mutant gliomas to zotiraciclib (ZTR).

Methods: We examined ZTR-induced cell death, mitochondrial dysfunction, and biogenesis defect at RNA, protein, and cellular levels. The survival benefit and pharmacodynamics of ZTR were evaluated using mouse models bearing mutant or wildtype IDH.

Results: The IC_{50} of ZTR in IDH-mutant patient-derived glioma cells was more than 50% lower than in IDH-wildtype cells. A high-throughput drug screen, utilizing a library of 2,481 approved and investigational drugs, provided independent evidence that ZTR was one of the most effective agents against IDH-mutant gliomas. ZTR-induced suppression of CDK9 and RNA Pol II phosphorylation was more pronounced in IDH-mutant cells. Low-dose ZTR (15 nM) suppressed mitochondrial respiration complexes and NAD+ production, leading to oxidative stress in IDH-mutant but not in IDH-wildtype cells. Furthermore, ZTR exposure resulted in a decrease in glycolysis, exacerbating bioenergetic failure. Finally, ZTR significantly prolonged the survival of mice bearing intracranial IDH-mutant gliomas but not in the IDH-wildtype counterpart. The combination of mitochondrial dysfunction and the inability to adapt to oxidative stress leads to potent ZTR-induced cell death and thereby an increased therapeutic vulnerability in IDH-mutant gliomas.

Conclusions: The findings led to the launch of a clinical trial of ZTR in IDH-mutant gliomas towards precision medicine (*NCT 05588141*).

Keywords: IDH-mutant, glioma, ZTR, CDK inhibitor, mitochondrial dysfunction

Introduction

Treating diffuse gliomas poses an immense challenge due to the inter-tumor heterogeneity of the disease and the limited availability of effective drugs with sufficient penetration into the central nervous system (CNS). The combination of temozolomide (TMZ) and radiation therapy, currently the standard treatment for newly diagnosed glioblastoma, represents one of very few successful treatment regimens for malignant primary brain tumors [1, 2]. However, a large phase III clinical trial (EORTC study 26053-22054) revealed that this standard treatment for glioblastoma, which are primarily IDH-wildtype tumors, does not provide additional benefit compared to radiation alone followed by adjuvant TMZ in newly diagnosed anaplastic astrocytoma, which are primarily IDH-mutant tumors [3]. Furthermore, the survival advantage of adjuvant TMZ to radiation alone is limited to those with *IDH* mutation, suggesting that the clinical benefit relies on the *IDH* mutation status in high-grade astrocytoma [3]. The diverse clinical responses to the same treatment in subsets of histologically similar but molecularly distinct gliomas underscore the significance of targeted therapy based on the genetic and molecular characteristics and the unique biology of the tumor. Therefore, treating specific subsets of gliomas with therapeutic vulnerability to a targeted therapy may lead to improved tumor control.

Zotiraciclib (ZTR, TG02) is a pyrimidine-based multi-kinase inhibitor with inhibitory effects on the cyclin-dependent kinases (CDKs), primarily CDK9, and regulates transcriptional processes in multiple cancer cell models [4]. The previous clinical trials have investigated ZTR and demonstrated its safety profiles [5, 6]. Our studies have shown that ZTR modulates various mechanisms of cancer cell survival in glioblastomas [7]. ZTR suppressed both transcription and expression of antiapoptotic genes, leading to cell death in glioblastoma cells. Additionally, ZTR induced mitochondrial dysfunction and depletes cellular ATP. Importantly, this provided evidence to support the ability of ZTR to cross the blood brain barrier (BBB), a prerequisite for targeting CNS related tumors including gliomas [7]. Encouraged by these promising preclinical studies, a phase I clinical trial of ZTR in combination with TMZ was conducted for patients with recurrent high-grade glioma [5]. Based on both preclinical and clinical evidence, the US Food and Drug Administration (FDA) granted orphan drug designation to ZTR as a therapy for malignant gliomas. Preliminary analysis of clinical outcomes revealed a statistically significant

improvement in progression-free survival (PFS) among patients with IDH-mutant gliomas compared to those with IDH-wildtype gliomas. While a better PFS in patients with IDH-mutant gliomas may indicate a more favorable prognosis, other studies have suggested an accelerated disease progression after the initial recurrence, diminishing the prognostic value of an *IDH* mutation after the first disease progression [8]. Most participants in this study were enrolled at their second recurrence at enrollment, suggesting a selective ZTR-related response in IDH-mutant gliomas.

The *IDH* mutation is a crucial genetic feature found in a subset of adult diffuse gliomas, which has distinct tumor biology and is utilized in the WHO classification of diffuse gliomas [9]. Wildtype IDH converts isocitrate to α-ketoglutarate, generating NADPH, while the IDH-mutant enzyme produces the oncometabolite 2-hydroxyglutarate (2-HG) and consumes NADPH [10, 11]. Due to reduced α-ketoglutarate levels, accumulation of 2-HG, and depletion of NADPH, IDH-mutant gliomas exhibit distinct biological characteristics, including redox imbalance, altered DNA damage repair, and heightened reliance on mitochondrial function for ATP production [12-14]. These unique features of IDH-mutant gliomas create potential vulnerabilities to specific drugs that modulate tumor metabolism. Building upon the promising clinical activity of ZTR and a mechanistic rational for targeting glioma vulnerability, we aimed to investigate the selective use of ZTR in gliomas harboring *IDH* mutations. In this study, we present preclinical evidence supporting the use of ZTR in patients with IDH-mutant gliomas. If the therapeutic vulnerability to ZTR can be demonstrated, ZTR may be utilized as a monotherapy to provide effective tumor control with reduced systemic toxicity.

Materials and Methods

Cell culture and reagents

GSC923 and GSC827 were generated from patients' glioblastoma tissues and cultured as previously reported [7]. TS603 was obtained from Dr. Timothy Chan, Memorial Sloan Kettering Cancer Center, New York, NY [15]. BT142 was purchased from ATCC and cultured as per instructions. NPA (shp53/shATRX/wtIDH1) and NPAI (shp53/shATRX/mIDH1^{R132H}), mice-derived neurosphere cell lines, were provided by Dr. Maria G. Castro, University of Michigan Medical School, Ann Arbor, MI [14]. Isogenic U87 (U87^{wt}, U87^{C8} (IDH-mutant) and U87^{C44}

(IDH-mutant)) and GBM1 ($GBM1^{wt}$ and $GBM1^{mut}$ (IDH-mutant)) cell lines were provided by Dr. Shuli Xia, Johns Hopkins University School of Medicine, Baltimore, MD [16]. Briefly, the glioma stem-like cells were cultured in neurobasal-A medium or DMEM/F12 medium supplemented with bFGF, EGF, N2, B27, and penicillin/streptomycin at 37°C with 5% CO_2. Adherent cell lines were cultured in DMEM medium supplemented with 10% FBS and 1% Penicillin/Streptomycin as previously reported [7].

Cell viability assay

A total of 1×10^5 cells/well were plated in geltrex precoated 12-well plates and treated with ZTR for 72 hours prior to cell counting using a Beckman Coulter ViCELL TM XR cell viability analyzer or Celigo Imaging Cytometer (Nexcelom Bioscience).

High-throughput drug screening

Six patient-derived glioma stem-like cell lines with *IDH1* mutations (GSC403L, GSC403H, BT142, MGG152, SF10602, and TS603) were screened with a cytotoxicity assay (48 hours Cell Titer-Glo) versus the MIPE 5.0 library (2481 agents: approved and investigational drugs with known MOA), as described and reported previously [17, 18]. Area under the curve (AUC) was utilized for ranking drug potency. For each compound tested, AUC values were averaged across the six cell lines and then normalized to Z-scores. MPO scores were plotted against Z-scores. Compounds of interest were highlighted based on a MPO score greater than 4 and an AUC Z-score of less than -3.

ROS measurement

ROS was measured using ROS-Glo H_2O_2 assay kit (Promega). Briefly, 1×10^4 cells/well were plated in geltrex pre-coated 96-well plates and treated with ZTR. H_2O_2 substrate solution was added in the culture medium and incubated for 6 hours. After adding ROS-Glo detection solution and incubating for 20 minutes, luminescence signal was read by the POLARStar Optima plate reader. The raw value was normalized to the protein content.

Caspase 3/7 activity assay

Caspase 3/7 cleavage activity was measured by Caspase-Glo 3/7 Assay Kit (Promega). 1 $\times 10^4$ cells/well were plated in a pre-coated 96-well plate. After treatment with ZTR for 72 hours, all wells were incubated with an equal volume of Caspase-Glo 3/7 reagent for 30 minutes and the luminescence signal was read by POLARStar Optima plate reader.

Cell apoptosis assay

The ZTR-treated cells were differentially stained with APC Annexin V (BD Biosciences) and propidium iodide (PI) followed by flow cytometry analysis performed based on the manufacturer's protocol. The fluorescence signal was measured by a BD LSRFortessa SORP I flow cytometer within 1 hour of staining and the percentage of apoptotic cells was quantified by FlowJo.

Western blot

Cells were treated with ZTR at 15 nM prior to the cell harvest. The cell lysates were processed with ice-cold RIPA lysis buffer supplemented with protease and phosphatase Inhibitor Cocktail (Thermo Fisher Scientific). Protein concentration was determined by a DC Protein Assay kit (Bio-Rad) and the same amount of protein was resolved by NuPAGE 4%-12% Noves Bis-Tris gels (Invitrogen). Proteins were transferred to nitrocellulose membranes (Bio-Rad) and probed with primary antibodies (diluted 1:1000) at 4°C overnight. After secondary antibody incubation and washing, membranes were visualized using ChemiDoc imaging system (Bio-Rad).

DNA fragmentation assay

Two million cells were treated with DMSO or 15nM of ZTR for 48 hours. DNA was extracted using the DNeasy Blood & Tissue kit (Qiagen) and total DNA concentration was determined by NanoDrop 8-Sample Spectrophotometer. Five hundred nanogram of DNA samples were resolved by electrophoresis in 10% Novex TBE gel (Invitrogen). The gel was stained by SYBR Gold DNA dye for 20 minutes and visualized by the ChemiDoc Imaging system (Bio-Rad).

MitoTracker Green FM staining

Cells were seeded in pre-coated 8-well glass coverslip (BD Biosciences) and treated with DMSO or 15nM ZTR for 48 hours. After removing media from the coverslip, prewarmed staining

solution with MitoTracker Green FM (100 nM, Thermo Fisher Scientific) was added for 30 minutes incubation at 37°C. After staining nuclei with Hoechst 33342, cells were observed using a NIKON confocal microscope.

Blue native polyacrylamide gel electrophoresis and complex I in-gel activity assay

Cells were collected, washed with PBS, and homogenized in the sample buffer, supplemented with 1% digitonin. After centrifuging the cell lysate at 20,000 g for 30 min at 4°C, supernatant was collected and aliquoted for further assay. Protein concentration was measured by the DC Protein Assay kit (Bio-Rad) and the same amount of sample was mixed with sample buffer, 5% G-250 Sample Additive, and deionized water for native gel electrophoresis in dark blue cathode buffer. When gel electrophoresis was done, the gel was fixed in 40% methanol, 10% acetic acid buffer, and then the gel was washed in destain buffer (8% acetic acid) until the background was washed off for visualization by ChemiDoc Imaging system (Bio-Rad).

For complex I in-gel activity assay, after gel electrophoresis in light blue cathode buffer, the gel was incubated in fresh complex I substrate buffer (2 mM Tris·Cl, 0.1 mg/ml NADH, 2.5 mg/ml Nitrotetrazolium Blue chloride) for 20 min [19]. The reaction was stopped by 10% acetic acid and the gel was washed with water for visualization by ChemiDoc Imaging system (Bio-Rad).

Mitochondrial respiration and ATP real-time measurement assay

Mitochondria respiration and real-time ATP production was assessed by Seahorse XF Cell Mito Stress Test Kit (Agilent) and Seahorse XF Real-Time ATP Rate Assay Kit (Agilent), respectively. Briefly, cells were plated at a density of 40,000 cells/well in the pre-coated Seahorse cell culture plates. After cells were attached and stabilized, cells were treated with DMSO or ZTR for 24 hours. Medium in all wells was replaced by the XF based assay medium supplemented with 10mM glucose, 10mM sodium pyruvate and 2mM glutamine. After loading to the Seahorse XF96 analyzer (Agilent), compounds included in the Mito Stress Test Kit (oligomycin, FCCP and Rot/AA) or Real-Time ATP Rate Assay Kit (oligomycin and Rot/AA) were injected according to the pre-set programs for measurement.

Transmission electron microscope (TEM) assay

GSC923 and TS603 cells were treated with DMSO or 15nM ZTR for 48 hours treatment for further TEM assay as previously described [20]. Briefly, each sample in an individual well in the form of adherent cells was pre-fixed prior to be processed for TEM analysis. All samples were stained with 1% Osmium Tetroxide and 0.5% Uranyl Acetate successively and then were dehydrated and kept in 100% pure resin for infiltration overnight. Samples would be polymerized, and ultra-thin sectioned with Leica UC6 Microtome with 70-80 nm thickness and picked up on 150-Cu mesh grid. Following post-staining with 50:50 (0.5% Uranyl Acetate:70% Ethanol), samples would be carbon coated and then imaged by Hitachi TEM microscope H7600, with bottom mount camera at HV: 80.0kv for TEM analysis.

RNA sequencing

GSC923 and TS603 cells were treated with DMSO or 15nM ZTR and collected after 24 or 48 hours. Total RNA was extracted using RNeasy Mini Kit (Qiagen) and passed the quality control of the Agilent RNA ScreenTape system. mRNA-Seq samples were pooled and sequenced on NextSeq 2000 P3 using TruSeq Stranded mRNA Kit and paired-end sequencing. Reads were aligned to the reference genome hg38 and gene expression levels were quantified using STAR and RSEM tools. Raw RNA-Seq data filtered via the filter by expression function from the Edger package [21] was normalized with the default DESeq2 workflow [22]. DESeq2 rlog transformed counts were filtered for protein coding genes only. Enrichment analysis was performed using Gene Set Enrichment Analysis (GSEA) on the filtered rlog counts with the Signal2Noise ranking metric [23]. The Hallmark, Reactome, Kegg, and Gene Ontology biological process collections within the Molecular Signatures Database (MSigDB) were analyzed for enrichment with the GSEA algorithm [24]. Only enriched gene sets with an FDR value less than .05 were considered for further analysis.

Syngeneic and xenograft orthotopic murine models of glioma

All the animal experiments were reviewed and approved by National Cancer Institute (NCI) Animal Use and Care Committee. Both syngeneic and xenograft orthotopic glioma mouse models were created to evaluate the treatment effect of ZTR in IDH-mutant and IDH-wildtype gliomas. To generate syngeneic model, isogenic cell line NPA (IDH-wt) or NPAI (IDH-mut) were injected (50,000 cells/2 μL) into the striatum of 8-weeks old C57BL/6 albino mice using a

stereotactic device (coordinates, 2mm anterior and 2mm lateral from bregma, and 2.5 mm depth from the dura). Animals bearing IDH-mutant and IDH-wildtype tumors were randomized into two groups based on body weights (n=7 mice for each group). Seven days after tumor implantation, ZTR (30mg/kg, i.p.) was administered twice a week for 21 days. To generate xenograft orthotopic model of gliomas with and without *IDH* mutation, isogenic cell line GBM1-wildtype or GBM1-mutant (100,000 cells/2 μl) were injected into 7-week-old female athymic (nu/nu) mice as previously described [25]. Two weeks after injection, ZTR treatment (30mg/kg, i.p.) was administered, twice a week for 10 weeks. Animal behavior and body weight were monitored constantly. Animals were euthanized when they reached the endpoints. Tumor tissues were collected to analyze PD markers after treatment. Kaplan-Meier analysis was performed to determine the survival curve.

Statistical analysis

Statistical analysis was performed using GraphPad Prism software using Student's *t*-Test or one-way ANOVA test followed by Student's t-Test as the post-statistical analysis. All tests were two-sided, and the results were shown as mean ± SEM or SD. A p-value less than 0.05 was considered as statistically significant. *, $P < 0.05$; **, $P < 0.01$; ***, or $P < 0.001$.

Results

Zotiraciclib demonstrates superior efficacy in IDH-mutant glioma cells

To demonstrate the superior efficacy of ZTR in IDH-mutant gliomas, we evaluated the cell viability of a panel of glioma cells with and without *IDH* mutations after treatment with ZTR. Firstly, using patient-derived glioma stem-like cell models, we observed a lower half maximal inhibition concentration (IC_{50}) of ZTR in IDH-mutant cells (TS603=7.06 nM and BT142=9.00 nM), compared to IDH-wildtype cells (GSC923=31.95 nM, GSC827=23.53 nM) (Figure 1Aa). In a pair of patient-derived adherent IDH-wildtype (U251) and IDH-mutant (HT1080) cells, HT1080 exhibited a lower IC_{50} of 35.94 nM compared to 66.13 nM in U251 when treated with ZTR (Figure 1Ab). Furthermore, we assessed the ZTR IC_{50} in mouse and patient-derived isogenic cell lines (NPA=30.73 nM/NPAI=17.65 nM, U87-wt=121.8 nM/U87-C8-mutant=71.6 nM /U87-C44-mutant=96.2 nM and GBM1-wt=23.13 nM/GBM1-mutant=16.95 nM).

Consistently, IDH-mutant cells displayed a lower IC_{50} compared to the isogenic IDH-wildtype cells, indicating increased sensitivity to ZTR in the IDH-mutant cells (Figure 1A c-e). *IDH1* mutation status was confirmed in all cell lines (Suppl. Figure 1A). To further support the investigation of ZTR in IDH-mutant glioma, we conducted a large high-throughput screen of 2,481 FDA-approved and investigational drugs using six primary patient-derived glioma cell lines with *IDH1* mutations [17]. ZTR was found to be one of six drugs showing both high efficacy and capacity to penetrate BBB (MPO>4 and AUC Z-score<-3), indicating ZTR is one of the most effective agents among all screened compounds that can be used in patients treating IDH-mutant gliomas (Figure 1B).

To investigate the selective sensitivity of IDH-mutant vs IDH-wildtype cells to ZTR, we selected a lower dose (LD) of ZTR (15 nM) compared to the previous study that used 50 nM in patient-derived glioblastoma cells. Live-cell imaging analysis by IncuCyte revealed an enhanced suppression of cell proliferation in IDH-mutant cell lines (TS603 and BT142) following LD ZTR treatment, while no significant effect was observed in IDH-wildtype cells (GSC923 and GSC827) (Figure 2A). To explore the critical gene and pathway alterations induced by the LD ZTR, we performed RNA sequencing (RNA-seq). Pathway analysis using gene set enrichment analysis (GSEA) demonstrated a significant suppression of cell cycle-related pathways after 24 hours of treatment specifically in the IDH-mutant TS603 cell line, but not in the IDH-wildtype GSC923 cells (Figure 2B). Moreover, the suppression of cell cycle-related pathways was maintained even after extending ZTR treatment to 48 hours (Suppl. Figure 1B). To further elucidate the cellular adaptive response to cell proliferation/cell cycle suppression, we examined the expression of genes related to stress & toxicity pathway. The volcano plot revealed a greater number of differentially expressed genes in TS603 compared to GSC923 upon LD ZTR treatment for 24 and 48 hours, indicating an elevated level of induced stress by LD ZTR treatment in IDH-mutant glioma (Figure 2C).

ZTR suppresses mitochondrial complexes and induces mito-stress in IDH-mutant glioma cells

Mutant IDH is known to induce altered cell metabolism and increase dependence on oxidative mitochondrial metabolism [26, 27]. In our previous study, we demonstrated that ZTR induces

mitochondria dysfunction in glioblastoma cells [28]. To investigate ZTR-induced mitochondrial changes in IDH-mutant glioma, we conducted an experiment using MitoTracker Green FM labeling. The results showed a greater loss of mitochondrial mass in the IDH-mutant glioma cells after LD ZTR treatment compared to the IDH-wildtype glioma cells (Figure 3A). Next, we examined the impact of LD ZTR on mitochondrial respiration complexes. The expression of genes encoding complexes I-V and other pathway activity signature genes was suppressed by LD ZTR specifically in TS603 cells, but not in GSC923 cells (Figure 3B). Protein expression of most complexes was also decreased in IDH-mutant cells (TS603 and BT142) following LD ZTR treatment, as observed in native blue gel of the mitochondrial pellet (Figure 3C). To further confirm the suppression of complex activity, an in-gel activity assay for complex I was performed, revealing ZTR-induced activity suppression only in IDH-mutant TS603 and BT142 cells, but not in IDH-wildtype GSC923 and GSC827 cells (Figure 3D). Although there was a decrease in protein expression level after LD ZTR in GSC827 (Figure 3C), no change in activity was detected (Figure 3D). The suppressed activity of complexes led to a significant reduction in the oxygen consumption rate (OCR) in IDH-mutant cells, indicating decreased oxidative phosphorylation and increased oxidative stress. Surprisingly, the extracellular acidification rate (ECAR), which is expected to increase in stress responses, was reduced in IDH-mutant cells [29] (Figure 3E). The suppressive effect of glycolysis was also confirmed in the isogenic IDH-wildtype and -mutant models (Suppl. Figure 1C). Importantly, ATP production through mitochondrial respiration and glycolysis was significantly decreased in the IDH-mutant cells, suggesting severe bioenergetic failure after LD ZTR treatment (Figure 3F).

ZTR-induced mito-stress intensifies the imbalance of redox pathway in IDH-mutant glioma cells

Previous studies have shown that NAD levels are decreased in IDH-mutant gliomas due to suppression of NAD salvage pathway enzymes [30]. The deficiency in complex I induced by ZTR may further interrupt the NAD/NADH balance. In our IDH-mutant cell model, we observed a lower baseline level of NAD expression compared to the IDH-wildtype cell (Figure 4A and Suppl. Figure 1D), which is consistent with the previous findings[30]. While ZTR-induced NAD suppression was observed in both IDH-mutant and IDH-wildtype cells, the decrease in NAD levels was much more pronounced in IDH-mutant gliomas upon ZTR treatment (Figure 4A).

Nicotinamide phosphoribosyltransferase (NAMPT) and nicotinate phosphoribosyltransferase domain containing 1 (NAPRT1) are two major rate-limiting enzymes involved in NAD synthesis that determine NAD levels. The NAMPT activity assay showed that ZTR did not suppress NAMPT activity up to a concentration of 50 nM, while a positive control, FK866, significantly reduced NAMPT activity (Figure 4B). Protein expression of NAMPT and NAPRT1 was not affected by LD ZTR treatment, suggesting that the reduction in NAD induced by ZTR is unlikely due to the suppression of NAMPT and NAPRT1. However, we observed a significant reduction in expression of poly (ADP-ribose) glycohydrolase (PARG) following LD ZTR in IDH-mutant glioma cells (Figure 4C). PARG is an enzyme involved in degrading ADP-ribose polymers to release NAD for re-use. The mechanism underlying the reduction in PARG is unclear, but it is hypothesized to contribute to the further reduction in NAD levels. In summary, LD ZTR reduced NAD levels in IDH-mutant glioma cells through the suppression of complex I and PARG. The impact of ZTR-induced NAD reduction was expected to be greater in IDH-mutant gliomas, which inherently have lower levels of NAD compared to IDH-wildtype gliomas.

Oxidative stress induced the production of mitochondrial reactive oxygen species (ROS) and disrupts redox homeostasis [31]. LD ZTR significantly increased ROS production in the IDH-mutant cells, indicating mito-stress after LD ZTR treatment (Figure 4D). To counterbalance the excessive ROS, a substantial amount of antioxidant is consumed, as evidenced by a significant decrease in GSH/GSSG ratio in IDH-mutant cells (Figure 4E). NADPH, which is critical for glutathione and thioredoxin systems to neutralize ROS, is largely consumed by 2-HG production in IDH-mutant cells [32] (Suppl. Figure 1D). LD ZTR treatment further reduced NADPH/NADP ratios to a greater extent in IDH-mutant cells compared to IDH-wildtype cells. In patient derived IDH-mutant GSCs, the NADPH/NADP ratio was downregulated by 30.3% and 40.5% in TS603 and BT142, respectively. However, there was only a 11.3% decrease in the IDH-wildtype GSC827 and no change in IDH-wildtype GSC923 (Figure 4F). The crucial enzymes G6PD and PGD, responsible for NADPH production, were not altered after ZTR treatment (Figure 4C). These results suggest that the low NADPH is likely caused by the increased consumption rather than decreased production of NADPH, thereby exacerbating the ROS imbalance in IDH-mutant gliomas.

As a cellular self-defense mechanism in response to increased ROS production, a group of genes encoding antioxidants is expected to be activated to eliminate excess ROS. However, the activity of antioxidant response element (ARE) luciferase, which reflects transcriptional activation of those genes, was found to be decreased rather than increased in IDH-mutant cells (Figure 4G). The mechanisms underlying this paradoxical reduction in ARE luciferase activity are unclear, but it further contributes to the redox imbalance. Excessive ROS production is a well-recognized mediator of induced DNA damage. In IDH-mutant cells, more genomic DNA fragmentation was observed compared to IDH-wildtype cells (Figure 4H). We further analyzed the enrichment of signaling pathways based on the RNA-seq data from GSC923 and TS603. While some DNA damage repair pathways were activated in both cell lines, TS603 showed evidence for suppression in other selected pathways. This indicates the suppression of DNA repair function specifically in IDH-mutant cells with LD ZTR treatment (Figure 4I). The ZTR-induced depletion of NAD, which serves as the substrate for the PARP signaling pathway, might further exacerbate the defect of DNA damage repair function, particularly in base excision repair, in IDH-mutant cells.

ZTR induced cell apoptosis and autophagy in IDH-mutant glioma cells

We previously demonstrated the suppression of RNA-Pol II and CDK9 activity in glioblastoma cells treated with ZTR at a concentration of 50 nM [7]. In this study, we observed a similar suppression in IDH-mutant, but not IDH-wildtype glioma cells, when treated with ZTR with a lower dose of ZTR (15 nM) (Figure 5A). The expression of short-lived anti-apoptotic proteins, namely MCL-1, XIAP and survivin, were also suppressed by LD ZTR in IDH-mutant cells (Figure 5Ba). Activation on c-PARP and γ-H2A.X further indicate the induction of DNA damage by LD ZTR in IDH-mutant cells, but not in IDH-wildtype cells (Figure 5Bb).

Caspase 3/7 activity, a biomarker of apoptosis, was significantly increased in IDH-mutant cells following LD ZTR treatment, while no significant change was observed in IDH-wildtype cells (Figure 5C). We further examined the activation of caspase 8 and caspase 9 at various time points. Activation of both intrinsic and extrinsic apoptosis pathways was demonstrated as early as 6-12 hours in ZTR-treated IDH-mutant cells (Figure 5D), suggesting the involvement of both pathways in early-stage apoptosis induced by LD ZTR. Apoptosis was further analyzed by flow cytometry, which showed an increase in the percentage of both early and late apoptotic cells in

LD ZTR-treated IDH-mutant cells, but not in IDH-wildtype cells (Figure 5Ea). Interestingly, a pan-apoptosis inhibitor, Z-VAD, only partially rescued the cell death (Figure 5Eb). These results suggest that apoptosis, a programed ATP-dependent cell death, is not the major type of cell death in ZTR-treated cells. Autophagy is considered an adaptive response to degrade organelles, including the mitochondria, under cell stress or damage [33]. In the IDH-mutant glioma cells, LD ZTR treatment induced the cleavage of autophagy marker LC3B (Figure 5F). To observe the cell morphological changes induced by ZTR, we also performed a transmission electron microscopy (TEM) examination in GSC923 and TS603 cells. In LD ZTR-treated IDH-mutant TS603 cells, mitochondria appeared dysmorphic and decreased in size. There was an increased number of double-membraned vesicles, varying in size and filled with digested materials, consistent with autophagy (Figure 5G). Other types of cell death, such as cell pyroptosis and necroptosis, were tested but were not detected in LD ZTR-treated cells (Suppl. Figure 1E).

ZTR is not a substrate for ABC multidrug transporters and confers survival benefit in IDH-mutant gliomas

ATP-binding cassette (ABC) transporter proteins, including P-glycoprotein transporters (Pgp, encoded by *ABCB1*), multidrug resistance-associated protein (MRP1, encoded by *ABCC1*), and ABC family member G2 (encoded by *ABCG2*) are known to transport a wide range of chemotherapies and targeted drugs, leading to cancer drug resistance [34]. To determine whether ZTR is a potential substrate of ABC transporter proteins, we investigated the treatment response to ZTR in cells overexpressing each of these three major transporter proteins. Cells transfected with ABCB1(MDR-19 cells), ABCG2(R-5 cells), and ABCC1 did not show any difference in response to ZTR treatment compared to cells transfected with empty vector pcDNA. However, these cells lines exhibited significant resistance to chemotherapeutic drugs known to be substrates of these transporters, such as mitoxantrone (Suppl. Figure 1F). These findings suggest that is unlikely to be a substrate for ABC transporter proteins. Since these ABC transporters play a crucial role in limiting the penetration into the brain at the blood-brain-barrier (BBB), this further provides evidence for ZTR to cross the BBB (Figure 6A). Next, we evaluated the efficacy of ZTR in syngeneic mouse models bearing orthotopic IDH-wildtype or IDH-mutant gliomas by intracranial implantation of NPA and NPAI cells, respectively. Seven days after the intracranial tumors were implanted, mice were treated with either vehicle or ZTR (Figure 6B). As expected,

mice bearing IDH-mutant gliomas survived longer than those with IDH-wildtype tumors. ZTR treatment prolonged survival significantly from 30 to 33 days in IDH-mutant cohort (p=0.01) (Figure 6C). However, a statistically significant survival benefit was not observed in ZTR treated IDH-wildtype group (18 vs 20 days, p=0.07). Tumor samples were collected when mice were euthanized at the endpoints. CDK9 phosphorylation was found to be suppressed in ZTR-treated mice compared to the DSMO-treated ones in the NPAI (IDH-mut) group but not in the NPA mice. This finding of a brain pharmacodynamic marker affected by ZTR further supports the BBB penetration of the drug. The expression of γH2A.X, an indicator of DNA damage, was observed in both IDH-wildtype and IDH-mutant groups following treatment but was more significant in the IDH-mutant group (Figure 6D). The survival benefit of ZTR treatment in IDH-mutant tumors was further confirmed in a xenograft murine glioma model (experimental 2) bearing isogenic GBM1-wildtype (65 vs 62 days, p=0.73) or GBM1-mutant (69 vs 76 days, p=0.03) cells (Figure 6B, E). Overall, ZTR prolonged the survival of mice bearing IDH-mutant gliomas. The findings of CDK9 activity suppression and DNA damage induction in tumor tissues from treated mice further support the BBB penetration of the drug and identified a potential pharmacodynamic biomarker for clinical investigation.

Discussion

In this study, we have provided evidence for the therapeutic vulnerability and the underlying mechanisms of action of ZTR in the treatment of IDH-mutant gliomas. We observed an increase in ZTR-induced cytotoxicity and suppression of cell proliferation in primary patient-derived glioma cells with mutant IDH compared to their counterparts with wildtype IDH. To further support the investigation of ZTR in clinical trials for IDH-mutant glioma patients, we conducted a high-throughput drug screen using a group of patient-derived IDH-mutant glioma cells. Among the 2,481 screened drugs, ZTR emerged as one of the top hits for inducing cytotoxicity while also having the ability to penetrate the BBB. Our study revealed that LD ZTR specifically targeted and suppressed mitochondrial complex activities in IDH-mutant gliomas. This disruption not only resulted in decreased NAD levels but also impaired ATP production in IDH-mutant gliomas, leading to mito stress. The inherent redox imbalance of IDH-mutant gliomas further contributed to the accumulation of ROS upon ZTR treatment. Additionally, ZTR interfered with the stress responses mechanisms of the IDH-mutant cells, compromising their

ability to relieve the stress-induced damage. By suppressing both of glycolysis and oxidative phosphorylation, ZTR caused severe bioenergetic failure in IDH-mutant gliomas. The compromised ROS clearance capability and deficient DNA damage repair mechanisms further potentiate DNA damage. Furthermore, ZTR suppressed the CDK9/RNA POLII phosphorylation pathway, resulting in decreased expression of antiapoptotic proteins such as MCL-1, survivin, and XIAP. This, in turn, induced apoptosis in IDH-mutant glioma cells. In summary, as illustrated in Figure 6F, ZTR induced bioenergetic failure, DNA damage, and apoptosis, ultimately leading to the death of IDH-mutant glioma cells. This study highlights the selective activities of ZTR in targeting IDH-mutant gliomas and underscores the importance of matching drug mechanisms of action with the underlying tumor biology to enhance precision medicine for brain tumor patients.

The impact of ZTR-induced mitochondrial stress on IDH-mutant glioma cells can be attributed to their unique metabolic vulnerability

Mutant IDH leads to the accumulation of 2-HG and rewiring the citric acid cycle metabolism, resulting in the enhanced reliance of IDH-mutant cells on mitochondrial oxidative phosphorylation for cellular energy production [12, 26]. Navis *et al*. have shown that increased mitochondrial density and activity in an IDH-mutant oligodendroglioma cells, indicating heightened mitochondrial metabolism in these cells [35]. Furthermore, accumulated 2-HG in IDH-mutant gliomas has been found to cause cell hypersuccinylation, leading to mitochondrial dysfunction [36]. The combination of increased dependence on mitochondrial metabolism and underlying mitochondrial dysfunction in IDH-mutant gliomas may explain their vulnerability to ZTR treatment, which further suppress the mitochondrial function [7, 37]. In our study, we observed that LD ZTR suppressed the expression of respiration complexes at both RNA and protein levels, inducing mito-stress. This treatment also resulted in an overall decrease in mitochondria mass in IDH-mutant glioma cells, disrupting oxidative phosphorylation and ATP production [29, 38, 39].

In addition to the reliance on mitochondria metabolism, IDH-mutant gliomas also exhibit a reduction in NAD levels due to the epigenetic downregulation of nicotinate phosphoribosyltransferase (Naprt1), an enzyme involved in NAD+ salvage pathway [30]. In our

study, LD ZTR treatment further suppressed NAD+ levels in the IDH-mutant cells, which contributes to impaired NAD+- mediated PARP DNA repair pathway. Rather than affecting NAMPT and NAPRT1, the rate-limiting enzymes of the NAD salvage pathway, ZTR was found to suppress the expression of PARG. PARG is responsible for the degradation of PAR chain and the removal of ADP-ribose moieties from modified proteins, thereby recycling NAD+ back into the system [40]. LD ZTR-induced PARG reduction may further contribute to the shortage of NAD in IDH-mutant glioma cells. Additionally, the mitochondrial complex I catalyzed the NADH oxidation and the elevation of NAD+, which is essential for energy production. The suppression of complex I activity by the LD ZTR treatment may partially contribute to the reduction of NAD induced by ZTR.

NADPH, another important molecule in the antioxidant system, plays a critical role in clearing up accumulated ROS. Depletion of NADPH results in the failure to effectively eliminate ROS, thereby potentiating oxidative stress [41]. In IDH-mutant glioma cells, the conversion of α-KG to 2-HG excessively consumes NADPH, resulting in an imbalance of redox homeostasis [42, 43]. LD ZTR treatment, by suppressing electron transport chain complex, particularly complex I, further increases ROS production and exacerbates the pre-existing redox imbalance, resulting in a more pronounced impact on IDH-mutant glioma cells.

ZTR suppressed several stress response pathways in IDH-mutant glioma cells

When cells are under mito-stress, glycolysis is expected to be upregulated to compensate for the loss of cellular energy [30]. However, in our study, we observed the opposite effect, with glycolysis being suppressed following LD ZTR, despite the already reduced oxidative phosphorylation in IDH-mutant cells. This suppression in glycolysis may be attributed to the depletion of NAD depletion or the inhibition of glycolytic enzymes by ROS [40, 41]. The simultaneous suppression of both oxidative phosphorylation and glycolysis by ZTR resulted in a severe bioenergetic failure in IDH-mutant gliomas. This disruption of energy metabolism further contributes to the vulnerability of IDH-mutant gliomas to ZTR-induced cytotoxicity.

In response to the increased ROS production, cells typically activate the ROS scavenger systems, such as the GSH/GSSG system and NADPH /NADP to restore redox balance. Additionally,

ARE plays a crucial role in mediating transcriptional activation of genes involved in detoxification and cytoprotection under oxidative stress [44]. However, in our study, despite the presence of oxidative stress, LD ZTR treatment failed to activate ARE in IDH-mutant glioma cells. The reasons underlying this suppression are not yet clear, but it suggests a failure to restore redox balance following LD ZTR treatment. Consequently, the excessive accumulation of ROS resulted in multiple oxidative cellular damage, including DNA damage [45]. Moreover, IDH-mutant tumors are characterized by global DNA hypermethylation, which can lead to the downregulation of the DNA damage sensor and impaired DNA repair pathway [46]. This inherent DNA damage repair deficiency in IDH-mutant cells may further sensitize them to agents that induce DNA damage, such as ZTR. Consistent with this, our study observed the activation of DNA damage markers, γH2A.X and cleaved-PARP, and DNA fragmentation in LD ZTR-treated IDH-mutant cells.

The presence of *IDH* mutation in glioma cells has been shown to dynamically reprogram the transcriptome, leading to persistent downregulation of certain transcription factors [47]. Additionally, the widespread hypermethylation, particularly in the promoter regions and CpG islands close to the transcription start sites, occurs in IDH-mutant cells, resulting in the predominant suppression of gene transcription [48]. Therefore, the aberrant transcriptome of IDH-mutant tumors might further contribute to the vulnerability to ZTR-induced CDK9 and RNA POLII inhibition. We previously demonstrated that treatment with ZTR at a concentration of 50 nM led to a decrease in CDK9 and RNA POLII phosphorylation in IDH-wildtype GSC827 and GSC923 cells. However, when the dosage of ZTR was decreased to 15 nM, this suppression of transcription signaling was only observed in IDH-mutant cells and no longer detected in IDH-wildtype glioma cells.

Mutant IDH and the accumulation of 2-HG have been reported to induce apoptosis and autophagy in glioma cells, making them more susceptible to inhibition of the anti-apoptotic protein, Bcl-xl [49, 50]. In the context of this vulnerability, LD ZTR further decreased the expression of MCL-1, XIAP, and survivin in IDH-mutant glioma cells, while the same suppression was not observed in IDH-wildtype gliomas. This suggests that IDH-mutant cells are more sensitive to the downregulation of anti-apoptotic proteins by LD ZTR. Although apoptosis

and autophagy were observed in the cell death process, the inhibition of these processes alone was not sufficient to completely prevent cell death, indicating the involvement of other cell death mechanisms. While markers of pyroptosis and necroptosis were not detected in ZTR-treated glioma cells, including those with *IDH* mutations, other cell death mechanisms, such as ferroptosis-induced cell death, may be worth investigating.

Preclinical findings provided rationale for clinical investigation of ZTR in IDH-mutant gliomas

Indeed, the multiple mechanisms of action of ZTR contribute to its antiglioma effects, targeting various biological features of IDH-mutant gliomas. The treatment-induced mitochondrial dysfunction and transcriptional regulation target the inherent biological features of IDH-mutant gliomas, including increased dependence on oxidative phosphorylation, redox imbalance, and NAD reduction. The increased vulnerability to the specific mechanisms of action of ZTR has led to increased efficacy of the drug treatment in this subset of gliomas with *IDH* mutation. The selective sensitivity of IDH-mutant gliomas to ZTR was demonstrated in the *in vivo* experiments, where a statistically significant survival benefit was observed only in IDH-mutant tumors following ZTR. This highlights the therapeutic vulnerability of IDH-mutant gliomas to the specific mechanisms of actions of ZTR creates an opportunity to treat IDH-mutant glioma patients with ZTR as monotherapy at a lower dose, thereby reducing the drug toxicity and improving the patients' quality of life.

Acknowledging the limitations of the study is crucial for the interpretation of the results and the development of future research. The mechanism of mitochondrial complex suppression by ZTR remains an area that requires further investigation. Understanding how ZTR affects the transcription of mitochondrial complexes, potentially through the inhibition of CDK9/RNA Pol II, would provide valuable insights into the drug's mode of action and its impact on cellular metabolism. Another limitation is the modest survival benefit observed in IDH-mutant glioma mouse models when ZTR was administered as a single agent. Although the survival prolongation was statistically significant, the improvement was approximately 10%, which may be considered modest. It is important to consider that the mouse models used in the study have a more aggressive disease course compared to clinical IDH-mutant gliomas. In a clinical setting, IDH-

mutant gliomas generally have a less aggressive disease course than their IDH-wildtype counterparts, allowing for a longer therapeutic window and potentially greater survival benefits. Additionally, considering combination therapies, such as combining ZTR with radiation, may enhance the therapeutic efficacy and improve patient outcomes. To address these limitations and further explore the potential of ZTR as a treatment option, ongoing clinical trials have been initiated. These clinical studies will provide valuable data on the efficacy and safety of ZTR in patients with IDH-mutant gliomas.

In conclusion, this study has shed light on the therapeutic potential of ZTR in targeting IDH-mutant gliomas. We first demonstrated the findings that highlight the ability of ZTR to disrupt mitochondrial function, suppress stress response pathways, and induce cell death specifically in IDH-mutant gliomas with a low concentration. Based on these promising results, a clinical study has been initiated to evaluate the efficacy and safety of ZTR as a monotherapy in IDH-mutant glioma patients (*NCT 05588141*). By exploiting the inherent vulnerabilities of IDH-mutant gliomas and leveraging the unique mechanisms of actions of ZTR, this therapeutic approach holds potential to provide effective tumor control while minimizing treatment toxicities.

Funding: This study is supported by the National Institutes of Health Intramural Research Program and Lasker Clinical Research Scholars Program.

Conflict of Interest: The authors declare no potential conflicts of interest.

Author contributions: Conceptualization, J.W., Y.P.; methodology, J.W., Y.P., G.Y., Z.S., F.J.N., M.R.G., M.M.G., M.G.C., Z.L., J.K. and C.J.T.; investigation, J.W., Y.P., G.Y., Z.S., Q.L., X.S., H.W., O.K., A.R., M.M., B.O., R.W.R., F.S., B.T., M.Z., H.S. W.Z. and D.D.; statistical analyses, J.W., Y.P., and Z.S.; writing – original draft, J.W. and Y.P., writing – review & editing, J.W., Y.P., Z.S., O.K., R.W.R., M.R.G., M.M.G., M.G.C., J.K. and C.J.T.; funding acquisition, J.W.; supervision, J.W.
All authors read and approved the final article and take responsibility for its content.

Data Availability: Data will be made available upon reasonable request.

References

1. Fernandes, C., et al., *Current Standards of Care in Glioblastoma Therapy*, in *Glioblastoma*, S. De Vleeschouwer, Editor. 2017: Brisbane (AU).
2. Stupp, R., et al., *Effects of radiotherapy with concomitant and adjuvant temozolomide versus radiotherapy alone on survival in glioblastoma in a randomised phase III study: 5-year analysis of the EORTC-NCIC trial.* Lancet Oncol, 2009. **10**(5): p. 459-66.
3. van den Bent, M.J., et al., *Adjuvant and concurrent temozolomide for 1p/19q non-co-deleted anaplastic glioma (CATNON; EORTC study 26053-22054): second interim analysis of a randomised, open-label, phase 3 study.* Lancet Oncol, 2021. **22**(6): p. 813-823.
4. Goh, K.C., et al., *TG02, a novel oral multi-kinase inhibitor of CDKs, JAK2 and FLT3 with potent anti-leukemic properties.* Leukemia, 2012. **26**(2): p. 236-43.
5. Wu, J., et al., *Phase I Study of Zotiraciclib in Combination with Temozolomide for Patients with Recurrent High-grade Astrocytomas.* Clin Cancer Res, 2021. **27**(12): p. 3298-3306.
6. Roboz, G.J., et al., *Phase I dose escalation study of TG02 in patients with advanced hematologic malignancies.* Journal of Clinical Oncology, 2012. **30**(15).
7. Su, Y.T., et al., *Novel Targeting of Transcription and Metabolism in Glioblastoma.* Clin Cancer Res, 2018. **24**(5): p. 1124-1137.
8. Miller, J.J., et al., *Accelerated progression of IDH mutant glioma after first recurrence.* Neuro Oncol, 2019. **21**(5): p. 669-677.
9. Yan, H., et al., *IDH1 and IDH2 mutations in gliomas.* N Engl J Med, 2009. **360**(8): p. 765-73.
10. Badur, M.G., et al., *Oncogenic R132 IDH1 Mutations Limit NADPH for De Novo Lipogenesis through (D)2-Hydroxyglutarate Production in Fibrosarcoma Sells.* Cell Rep, 2018. **25**(4): p. 1018-1026 e4.
11. Dang, L., S. Jin, and S.M. Su, *IDH mutations in glioma and acute myeloid leukemia.* Trends Mol Med, 2010. **16**(9): p. 387-97.
12. Fack, F., et al., *Altered metabolic landscape in IDH-mutant gliomas affects phospholipid, energy, and oxidative stress pathways.* EMBO Mol Med, 2017. **9**(12): p. 1681-1695.
13. Miller, J.J., et al., *Isocitrate dehydrogenase (IDH) mutant gliomas: A Society for Neuro-Oncology (SNO) consensus review on diagnosis, management, and future directions.* Neuro Oncol, 2023. **25**(1): p. 4-25.
14. Nunez, F.J., et al., *IDH1-R132H acts as a tumor suppressor in glioma via epigenetic up-regulation of the DNA damage response.* Sci Transl Med, 2019. **11**(479).
15. Rohle, D., et al., *An inhibitor of mutant IDH1 delays growth and promotes differentiation of glioma cells.* Science, 2013. **340**(6132): p. 626-30.
16. Ma, D., et al., *Mutant IDH1 promotes phagocytic function of microglia/macrophages in gliomas by downregulating ICAM1.* Cancer Lett, 2021. **517**: p. 35-45.
17. Mathews Griner, L.A., et al., *High-throughput combinatorial screening identifies drugs that cooperate with ibrutinib to kill activated B-cell-like diffuse large B-cell lymphoma cells.* Proc Natl Acad Sci U S A, 2014. **111**(6): p. 2349-54.

18. Lin, G.L., et al., *Therapeutic strategies for diffuse midline glioma from high-throughput combination drug screening.* Sci Transl Med, 2019. **11**(519).
19. Jha, P., X. Wang, and J. Auwerx, *Analysis of Mitochondrial Respiratory Chain Supercomplexes Using Blue Native Polyacrylamide Gel Electrophoresis (BN-PAGE).* Curr Protoc Mouse Biol, 2016. **6**(1): p. 1-14.
20. Greer, Y.E., et al., *ONC201 kills breast cancer cells in vitro by targeting mitochondria.* Oncotarget, 2018. **9**(26): p. 18454-18479.
21. Chen, Y., A.T. Lun, and G.K. Smyth, *From reads to genes to pathways: differential expression analysis of RNA-Seq experiments using Rsubread and the edgeR quasi-likelihood pipeline.* F1000Res, 2016. **5**: p. 1438.
22. Love, M.I., W. Huber, and S. Anders, *Moderated estimation of fold change and dispersion for RNA-seq data with DESeq2.* Genome Biol, 2014. **15**(12): p. 550.
23. Subramanian, A., et al., *Gene set enrichment analysis: a knowledge-based approach for interpreting genome-wide expression profiles.* Proc Natl Acad Sci U S A, 2005. **102**(43): p. 15545-50.
24. Liberzon, A., et al., *The Molecular Signatures Database (MSigDB) hallmark gene set collection.* Cell Syst, 2015. **1**(6): p. 417-425.
25. Tilghman, J., et al., *Regulation of Glioblastoma Tumor-Propagating Cells by the Integrin Partner Tetraspanin CD151.* Neoplasia, 2016. **18**(3): p. 185-98.
26. Grassian, A.R., et al., *IDH1 mutations alter citric acid cycle metabolism and increase dependence on oxidative mitochondrial metabolism.* Cancer Res, 2014. **74**(12): p. 3317-31.
27. Reitman, Z.J., et al., *Profiling the effects of isocitrate dehydrogenase 1 and 2 mutations on the cellular metabolome.* Proc Natl Acad Sci U S A, 2011. **108**(8): p. 3270-5.
28. Le Rhun, E., et al., *Profound, durable and MGMT-independent sensitivity of glioblastoma cells to cyclin-dependent kinase inhibition.* Int J Cancer, 2019. **145**(1): p. 242-253.
29. Olsen, R.K., N. Cornelius, and N. Gregersen, *Redox signalling and mitochondrial stress responses; lessons from inborn errors of metabolism.* J Inherit Metab Dis, 2015. **38**(4): p. 703-19.
30. Tateishi, K., et al., *Extreme Vulnerability of IDH1 Mutant Cancers to NAD+ Depletion.* Cancer Cell, 2015. **28**(6): p. 773-784.
31. Guo, C., et al., *Oxidative stress, mitochondrial damage and neurodegenerative diseases.* Neural Regen Res, 2013. **8**(21): p. 2003-14.
32. Gelman, S.J., et al., *Consumption of NADPH for 2-HG Synthesis Increases Pentose Phosphate Pathway Flux and Sensitizes Cells to Oxidative Stress.* Cell Rep, 2018. **22**(2): p. 512-522.
33. Glick, D., S. Barth, and K.F. Macleod, *Autophagy: cellular and molecular mechanisms.* J Pathol, 2010. **221**(1): p. 3-12.
34. Gottesman, M.M., et al., *Toward a Better Understanding of the Complexity of Cancer Drug Resistance.* Annu Rev Pharmacol Toxicol, 2016. **56**: p. 85-102.
35. Navis, A.C., et al., *Increased mitochondrial activity in a novel IDH1-R132H mutant human oligodendroglioma xenograft model: in situ detection of 2-HG and alpha-KG.* Acta Neuropathol Commun, 2013. **1**: p. 18.

36. Li, F., et al., *NADP(+)-IDH Mutations Promote Hypersuccinylation that Impairs Mitochondria Respiration and Induces Apoptosis Resistance.* Mol Cell, 2015. **60**(4): p. 661-75.
37. Chen, R., et al., *The multi-kinase inhibitor TG02 induces apoptosis and blocks B-cell receptor signaling in chronic lymphocytic leukemia through dual mechanisms of action.* Blood Cancer J, 2021. **11**(3): p. 57.
38. Yamamoto, M., H. Inohara, and T. Nakagawa, *Targeting metabolic pathways for head and neck cancers therapeutics.* Cancer Metastasis Rev, 2017. **36**(3): p. 503-514.
39. Mullarky, E. and L.C. Cantley, *Diverting Glycolysis to Combat Oxidative Stress*, in *Innovative Medicine: Basic Research and Development*, K. Nakao, N. Minato, and S. Uemoto, Editors. 2015: Tokyo. p. 3-23.
40. Harrision, D., et al., *Poly(ADP-Ribose) Glycohydrolase (PARG) vs. Poly(ADP-Ribose) Polymerase (PARP) - Function in Genome Maintenance and Relevance of Inhibitors for Anti-cancer Therapy.* Front Mol Biosci, 2020. **7**: p. 191.
41. Fernandez-Marcos, P.J. and S. Nobrega-Pereira, *NADPH: new oxygen for the ROS theory of aging.* Oncotarget, 2016. **7**(32): p. 50814-50815.
42. Dang, L., et al., *Cancer-associated IDH1 mutations produce 2-hydroxyglutarate.* Nature, 2009. **462**(7274): p. 739-44.
43. Ward, P.S., et al., *The common feature of leukemia-associated IDH1 and IDH2 mutations is a neomorphic enzyme activity converting alpha-ketoglutarate to 2-hydroxyglutarate.* Cancer Cell, 2010. **17**(3): p. 225-34.
44. Rushmore, T.H., M.R. Morton, and C.B. Pickett, *The antioxidant responsive element. Activation by oxidative stress and identification of the DNA consensus sequence required for functional activity.* J Biol Chem, 1991. **266**(18): p. 11632-9.
45. Srinivas, U.S., et al., *ROS and the DNA damage response in cancer.* Redox Biol, 2019. **25**: p. 101084.
46. Inoue, S., et al., *Mutant IDH1 Downregulates ATM and Alters DNA Repair and Sensitivity to DNA Damage Independent of TET2.* Cancer Cell, 2016. **30**(2): p. 337-348.
47. Turcan, S., et al., *Mutant-IDH1-dependent chromatin state reprogramming, reversibility, and persistence.* Nat Genet, 2018. **50**(1): p. 62-72.
48. Akalin, A., et al., *Base-pair resolution DNA methylation sequencing reveals profoundly divergent epigenetic landscapes in acute myeloid leukemia.* PLoS Genet, 2012. **8**(6): p. e1002781.
49. Gilbert, M.R., et al., *Autophagy and oxidative stress in gliomas with IDH1 mutations.* Acta Neuropathol, 2014. **127**(2): p. 221-33.
50. Karpel-Massler, G., et al., *Induction of synthetic lethality in IDH1-mutated gliomas through inhibition of Bcl-xL.* Nat Commun, 2017. **8**(1): p. 1067.

Figure legends

Figure 1. ZTR has selective cytotoxic effect on IDH-mutant glioma cells. A. The cytotoxic effect of ZTR in patient-derived stem-like glioma cells (a), patient-derived adherent tumor cells (b), isogenic mouse-derived cells (c), and isogenic human-derived cells (d-e). Cells were treated with serial dosages of ZTR for 72 hours prior to cell viability assay. B. In a high throughput drug screen of 2,481 FDA-approved and investigational drugs, the MPO score against average AUC Z-Score of six primary patient-derived glioma cell lines with *IDH1* mutations showing that ZTR (green dot) was one of the few agents having both high efficacy and capacity to penetrate BBB, defined as AUC Z-score<-3 and MPO>4, respectively.

Figure 2. ZTR suppresses proliferation and affects stress response in IDH-mutant glioma cells. A. Cell proliferation assay of patient-derived stem-like cells treated with 15 nM ZTR. Phase area confluence was measured every 3 hours by Incucyte up to 72 hours. All cell line data were normalized to its own start time point (0 hour) value. B. RNAseq results of GSC923 and TS603 cell lines showing enriched gene sets related to cell cycle processes after ZTR treatment at 15 nM for 24 hours. C. Volcano plots based on RNAseq results showing the mRNA level changes of a panel of stress & toxicity pathway related, differentially expressed genes after ZTR treatment at 15 nM for 24 or 48 hours. n=3.

Figure 3. ZTR suppresses mitochondrial complexes and induces mito-stress in IDH-mutant glioma cells. A. MitoTracker Green FM staining demonstrating the mitochondrial mass volume change after ZTR treatment at 15 nM for 48 hours in GSC923 (IDH-wildtype) and TS603 (IDH-mutant) cells. Scale bar=10 um. B. Profiler PCR arrays showing the mRNA level changes of the

signature genes coding for mitochondrial complexes and pathway activity after ZTR treatment at 15 nM for 48 hours, inGSC923 and TS603 cells. n=3. C. Native blue gel staining of mitochondrial complexes protein after ZTR treatment at 15 nM for 48 hours in IDH-wildtype (GSC923, GSC827) and IDH-mutant (TS603 and BT142) cells. D. In-gel activity assay showing the complex I activity changes after ZTR treatment at 15 nM for 48 hours. GAPDH was blotted as internal control. E. Mito-stress seahorse assay showing mitochondrial stress by measuring the OCR and ECAR after ZTR treatment at 15 nM for 24 hours. F. Real-time ATP seahorse assay measuring mitoATP and glycolATP production changes after ZTR treatment at 15 nM for 24 hours. *, $P < 0.05$; **, $P < 0.01$; ***, $P < 0.001$.

Figure 4. ZTR intensifies the imbalance of redox pathway in IDH-mutant glioma cells A. NAD-Glo assay measuring NAD level changes in NPA/I or GSC cells after ZTR treatment at 50 nM and 15 nM, respectively. The signals were measured after 48 hours' treatment. B. Cell-free NAMPT activity assay measuring NAMPT enzyme activity with different dose of ZTR treatment in time-dependent manner. FK866 was used as a positive control. C. Western blotting showing protein levels of NAD and NADPH related enzymes with and without ZTR treatment at 15 nM for 72 hours. GAPDH was blotted as internal control. D. ROS-Glo assay measuring the ROS level in NPA/I or GSCs cell lines with and without ZTR treatment at 50 nM and 15 nM, respectively. E. GSH/GSSG-Glo assay measuring the GSH/GSSG ratio changes in patient-derived GSCs cell lines following ZTR treatment at 15 nM. F. NADP/NADPH-Glo assay measuring NADP/NADPH changes in NPA/I or patient-derived GSC cells after ZTR treatment at 50 nM and 15 nM, respectively. G. ARE luciferase assay measuring the ARE activity changes in GSCs cell lines with ZTR treatment at 15 nM. H. Total genomic DNA electrophoresis analysis

showing DNA fragmentation after ZTR treatment at 15 nM for 48 hours. I. RNAseq results of GSC923 and TS603 cell lines showing significantly enriched gene sets related to DNA damage and repair processes after 24 hours ZTR treatment at 15 nM. *, $P < 0.05$; **, $P < 0.01$; ***, $P < 0.001$.

Figure 5. ZTR induces cell apoptosis and autophagy in IDH-mutant glioma cells. A. Western blotting showing CDK9 and RNA Pol II phosphorylation levels with ZTR treatment at 15 nM for 72 hours. β-actin was blotted as internal control. B. (a) Western blotting showing short-lived antiapoptotic protein expression levels with ZTR treatment at 15 nM for 48 hours. (b) Western blotting showing DNA damage repair protein expression levels with ZTR treatment at 15 nM for 72 hours. GAPDH was blotted as internal control. C. Caspase 3/7-Glo assay showing caspase 3/7 activity changes after ZTR treatment at 15 nM for 72 hours. D. Western blotting showing cleavage of caspase 9, 8 and 3 after ZTR treatment at 15 nM. Samples were collected after 0, 3-, 6-, 12-, and 24-hours treatment. β-actin was blotted as internal control. E. (a) Flow cytometry assay measuring the percentage of early/late apoptotic and necrotic cell by staining with APC Annexin V/PI after 15 nM ZTR or both 15 nM ZTR and 10 uM Z-VAD for 72 hours. DMSO treatment was used as the control. (b) Statistic analysis of early apoptotic ratio in all cell lines. F. Western blotting showing cleavage of autophagy markers, LC3B after ZTR treatment at 15 nM for 72 hours. GAPDH was blotted as internal control. G. Transmission electron microscope pictures showing the mitochondrial morphology change and presence of double-membraned vesicles, filled with digested materials (indicated by red arrows), consistent with autophagy in TS603 cells after ZTR treatment at 15 nM for 48 hours. Scale bar=500 nm.

Figure 6. Single agent ZTR confers survival benefit in IDH-mutant gliomas. A. ABC transporter assay showing that overexpression of R5, MDR-19 and MRP1, the common ABC multidrug transporters, does not affect ZTR efficacy, suggesting ZTR is unlikely to be the substrate of these ABC transporters. Cells carrying pcDNA were used as negative controls and the expression of the transporters was confirmed by FACS analysis and demonstration that they conferred resistance to other cytotoxic agents that were substrates for the transporters. B. Schematic illustration for the allograft (experimental 1) and xenograft (experimental 2) modeling and ZTR treatment schedule. C. Kaplan-Meier analysis of intracranial allograft in mice bearing NPA/NPAI cells that received ZTR treatment. D. (a) Western blotting showing protein expressions of CDK9, and RNA Pol II phosphorylation and γ-H2A.X from tumor tissues with or without ZTR treatment. GAPDH was blotted as internal control. (b) Statistic analysis of p-CDK9 and γ-H2A.X relative protein levels, which was normalized to β-actin. E. Kaplan-Meier analysis of intracranial xenograft in mice bearing GBM1-wt/-mutant cells that received ZTR treatment. F. A graphic summary illustrating the mechanisms selective sensitivity to ZTR in cells carrying *IDH* mutation.

Supplementary Figure 1. A. Western blotting and Sanger sequencing demonstrating the *IDH1* mutation status of all human- and mouse-derived cell lines. B. RNAseq results of GSC923 and TS603 cell lines showing enriched gene sets related to cell cycle processes after ZTR treatment at 15 nM for 48 hours. C. Mito-stress seahorse assay showing ECAR measurement after ZTR treatment at 50 nM for 24 hours in NPA and NPAI cells. D. Baseline levels of NAD and NADPH/NADP in NAP, NAPI and patient-derived GSC cell lines. E. Western blotting showing GSDMC, GSDMC and p-MLKL expression in all cell lines with ZTR treatment. F. ABC

transporter assay showing that cells with overexpressed R5, MDR-19 and MRP1, the common ABC multidrug transporters, were resistant to mitoxantrone, which was a known substrate of these transporters.

Figure 1

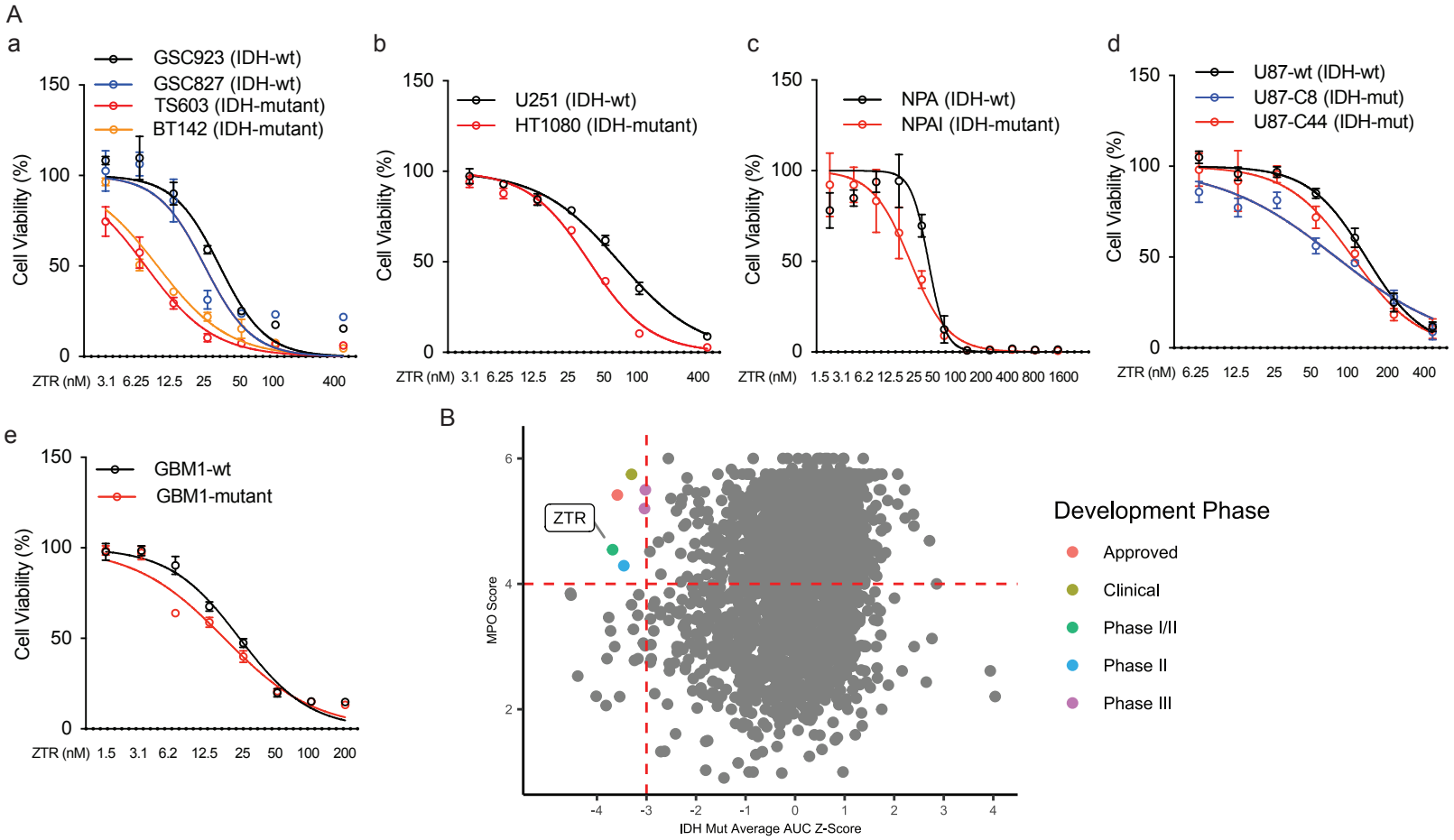
A
a
GSC923 (IDH-wt)
GSC827 (IDH-wt)
TS603 (IDH-mutant)
BT142 (IDH-mutant)
Cell Viability (%)
ZTR (nM) 3.1 6.25 12.5 25 50 100 400
b
U251 (IDH-wt)
HT1080 (IDH-mutant)
Cell Viability (%)
ZTR (nM) 3.1 6.25 12.5 25 50 100 400
c
NPA (IDH-wt)
NPAI (IDH-mutant)
Cell Viability (%)
ZTR (nM) 1.5 3.1 6.2 12.5 25 50 100 200 400 800 1600
d
U87-wt (IDH-wt)
U87-C8 (IDH-mut)
U87-C44 (IDH-mut)
Cell Viability (%)
ZTR (nM) 6.25 12.5 25 50 100 200 400
e
GBM1-wt
GBM1-mutant
Cell Viability (%)
ZTR (nM) 1.5 3.1 6.2 12.5 25 50 100 200
B
ZTR
MPO Score
IDH Mut Average AUC Z-Score
Development Phase
Approved
Clinical
Phase I/II
Phase II
Phase III

Figure 2

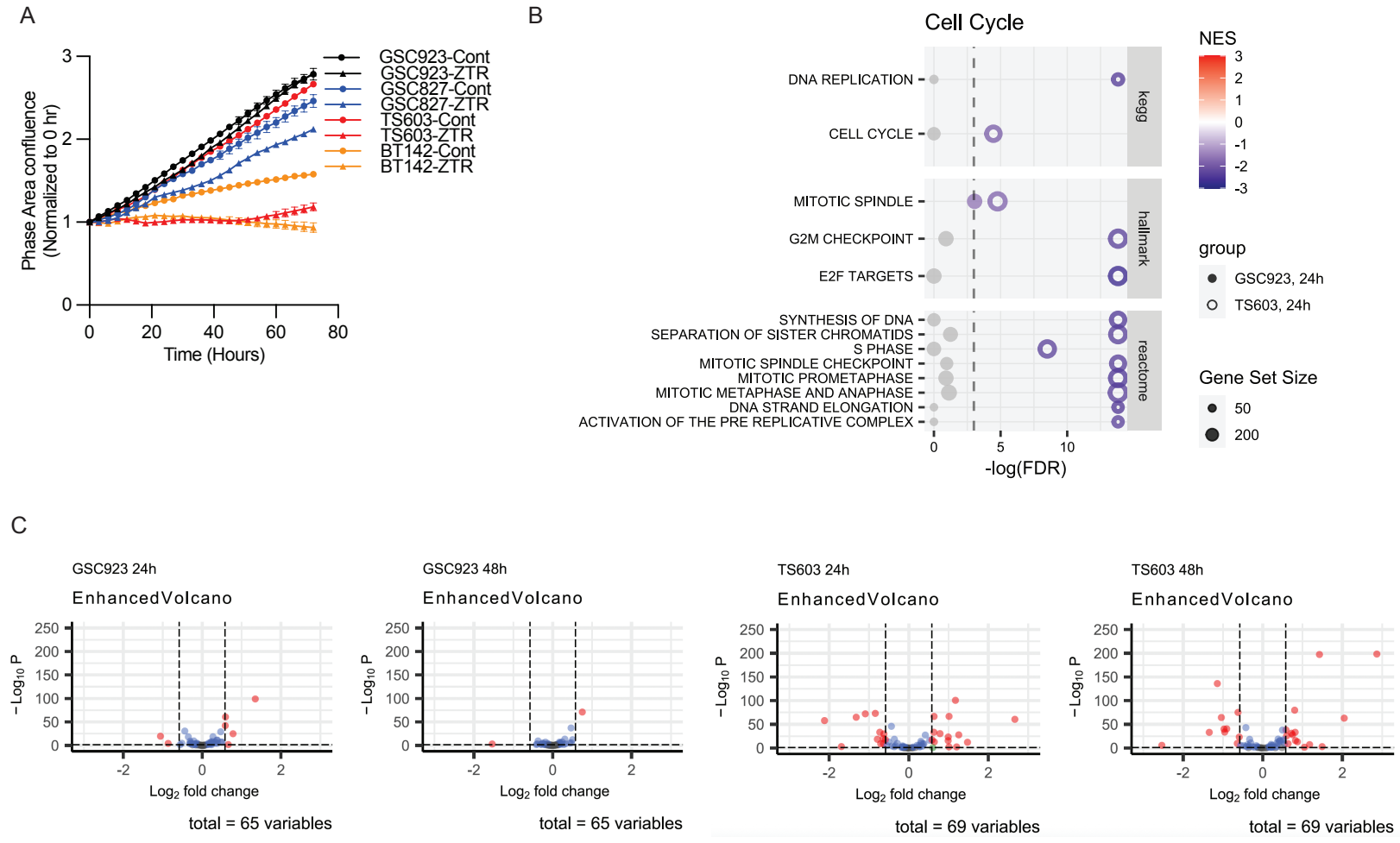
A
Phase Area confluence (Normalized to 0 hr)
Time (Hours)
GSC923-Cont
GSC923-ZTR
GSC827-Cont
GSC827-ZTR
TS603-Cont
TS603-ZTR
BT142-Cont
BT142-ZTR
B
Cell Cycle
DNA REPLICATION
CELL CYCLE
MITOTIC SPINDLE
G2M CHECKPOINT
E2F TARGETS
SYNTHESIS OF DNA
SEPARATION OF SISTER CHROMATIDS
S PHASE
MITOTIC SPINDLE CHECKPOINT
MITOTIC PROMETAPHASE
MITOTIC METAPHASE AND ANAPHASE
DNA STRAND ELONGATION
ACTIVATION OF THE PRE REPLICATIVE COMPLEX
kegg
hallmark
reactome
-log(FDR)
NES
group
GSC923, 24h
TS603, 24h
Gene Set Size
C
GSC923 24h
GSC923 48h
TS603 24h
TS603 48h
EnhancedVolcano
−Log10 P
Log2 fold change
total = 65 variables
total = 65 variables
total = 69 variables
total = 69 variables

Figure 3

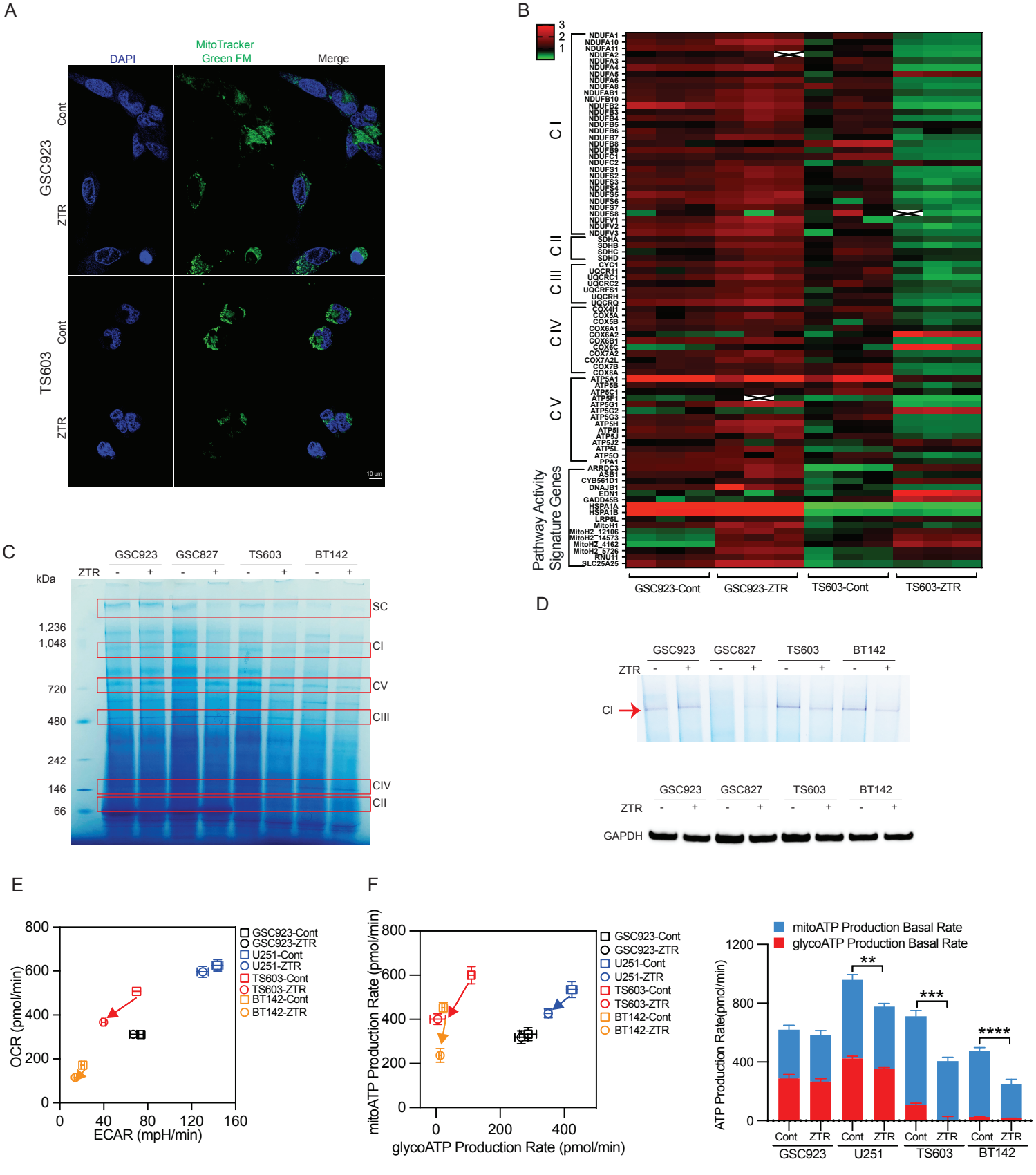
A
DAPI
MitoTracker Green FM
Merge
GSC923
Cont
ZTR
TS603
Cont
ZTR
10 um
B
3
2
1
C I
C II
C III
C IV
C V
Pathway Activity Signature Genes
GSC923-Cont
GSC923-ZTR
TS603-Cont
TS603-ZTR
C
GSC923
GSC827
TS603
BT142
ZTR
kDa
1,236
1,048
720
480
242
146
66
SC
CI
CV
CIII
CIV
CII
D
GSC923
GSC827
TS603
BT142
ZTR
CI
GAPDH
E
OCR (pmol/min)
ECAR (mpH/min)
GSC923-Cont
GSC923-ZTR
U251-Cont
U251-ZTR
TS603-Cont
TS603-ZTR
BT142-Cont
BT142-ZTR
F
mitoATP Production Rate (pmol/min)
glycoATP Production Rate (pmol/min)
mitoATP Production Basal Rate
glycoATP Production Basal Rate
ATP Production Rate(pmol/min)
Cont
ZTR
GSC923
U251
TS603
BT142

Figure 4

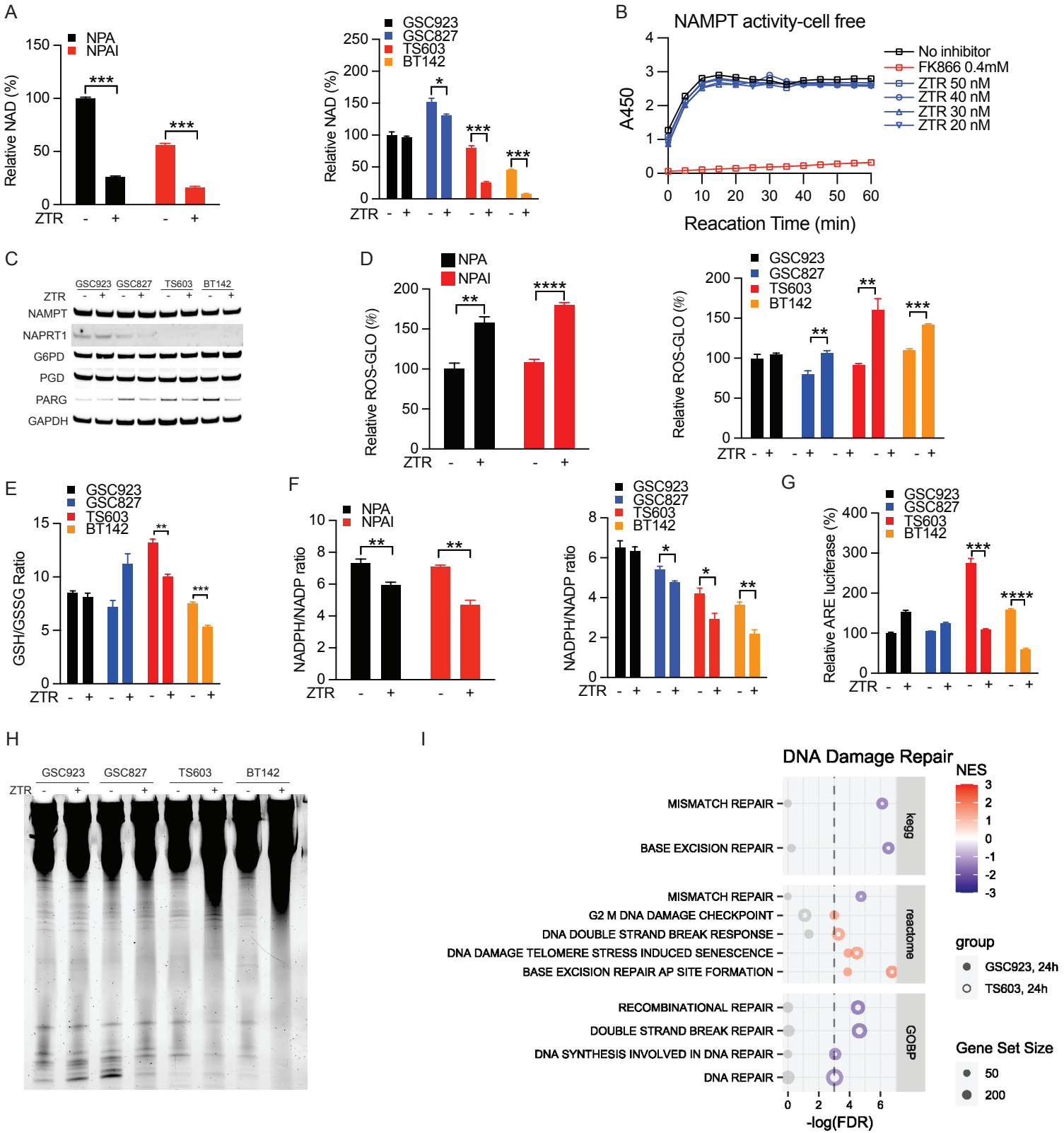
A
NPA
NPAI
Relative NAD (%)
ZTR
GSC923
GSC827
TS603
BT142
B
NAMPT activity-cell free
A450
Reacation Time (min)
No inhibitor
FK866 0.4mM
ZTR 50 nM
ZTR 40 nM
ZTR 30 nM
ZTR 20 nM
C
NAMPT
NAPRT1
G6PD
PGD
PARG
GAPDH
D
Relative ROS-GLO (%)
E
GSH/GSSG Ratio
F
NADPH/NADP ratio
G
Relative ARE luciferase (%)
H
I
DNA Damage Repair
MISMATCH REPAIR
BASE EXCISION REPAIR
kegg
G2 M DNA DAMAGE CHECKPOINT
DNA DOUBLE STRAND BREAK RESPONSE
DNA DAMAGE TELOMERE STRESS INDUCED SENESCENCE
BASE EXCISION REPAIR AP SITE FORMATION
reactome
RECOMBINATIONAL REPAIR
DOUBLE STRAND BREAK REPAIR
DNA SYNTHESIS INVOLVED IN DNA REPAIR
DNA REPAIR
GOBP
-log(FDR)
NES
group
GSC923, 24h
TS603, 24h
Gene Set Size
50
200

Figure 5

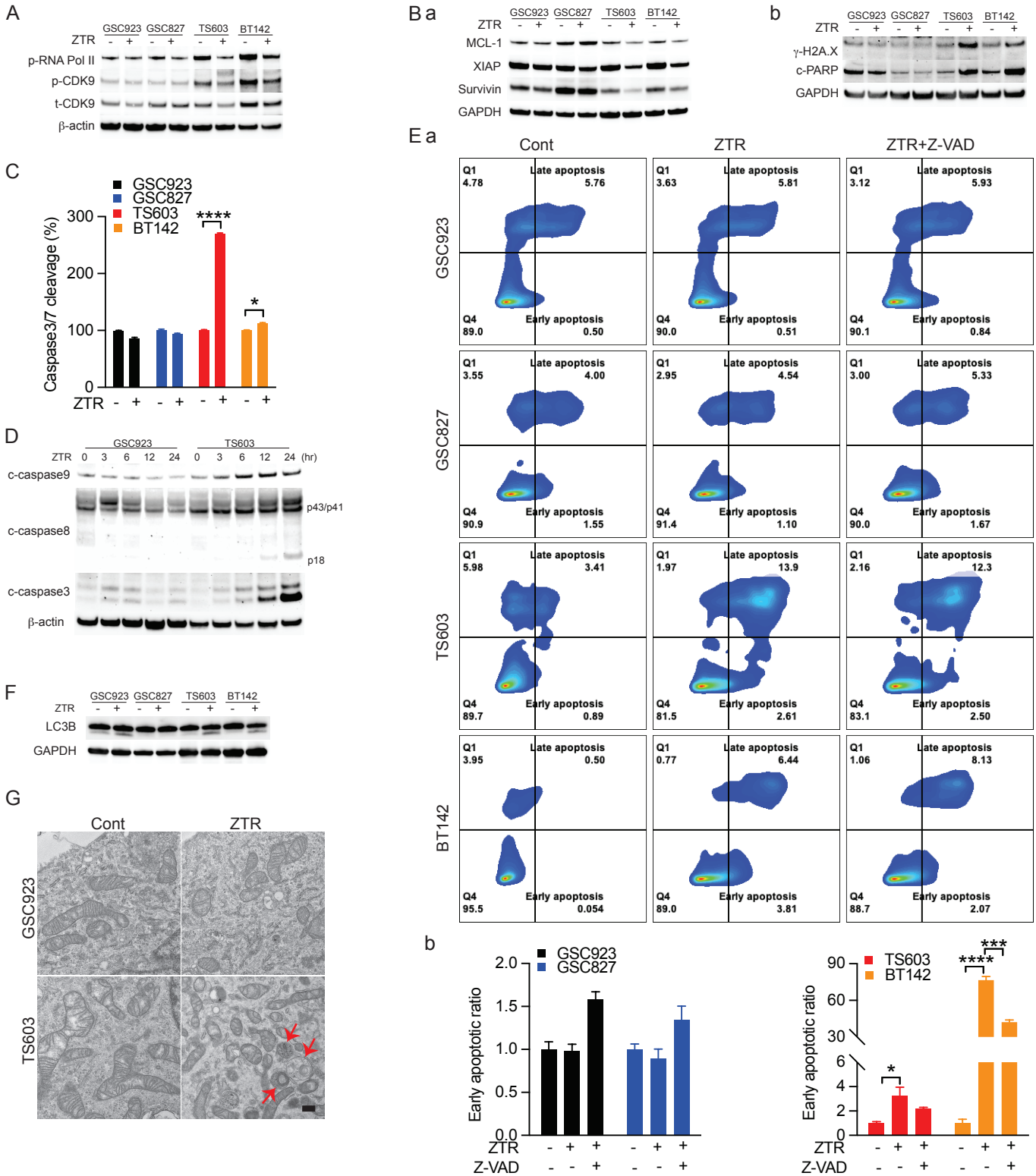
A
GSC923 GSC827 TS603 BT142
ZTR - + - + - + - +
p-RNA Pol II
p-CDK9
t-CDK9
β-actin
B a
GSC923 GSC827 TS603 BT142
ZTR - + - + - + - +
MCL-1
XIAP
Survivin
GAPDH
b
GSC923 GSC827 TS603 BT142
ZTR - + - + - + - +
γ-H2A.X
c-PARP
GAPDH
C
GSC923
GSC827
TS603
BT142
Caspase3/7 cleavage (%)
300
200
100
0
****
*
ZTR - + - + - + - +
D
GSC923 TS603
ZTR 0 3 6 12 24 0 3 6 12 24 (hr)
c-caspase9
p43/p41
c-caspase8
p18
c-caspase3
β-actin
E a
Cont
ZTR
ZTR+Z-VAD
GSC923
GSC827
TS603
BT142
Q1 Late apoptosis
Q4 Early apoptosis
4.78 5.76 89.0 0.50
3.63 5.81 90.0 0.51
3.12 5.93 90.1 0.84
3.55 4.00 90.9 1.55
2.95 4.54 91.4 1.10
3.00 5.33 90.0 1.67
5.98 3.41 89.7 0.89
1.97 13.9 81.5 2.61
2.16 12.3 83.1 2.50
3.95 0.50 95.5 0.054
0.77 6.44 89.0 3.81
1.06 8.13 88.7 2.07
F
GSC923 GSC827 TS603 BT142
ZTR - + - + - + - +
LC3B
GAPDH
G
Cont
ZTR
GSC923
TS603
b
GSC923
GSC827
Early apoptotic ratio
2.0
1.5
1.0
0.5
0.0
ZTR - + + - + +
Z-VAD - - + - - +
TS603
BT142
90
60
30
6
4
2
0
*
****
***
ZTR - + + - + +
Z-VAD - - + - - +

Figure 6

A

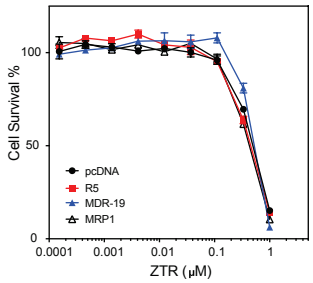

B

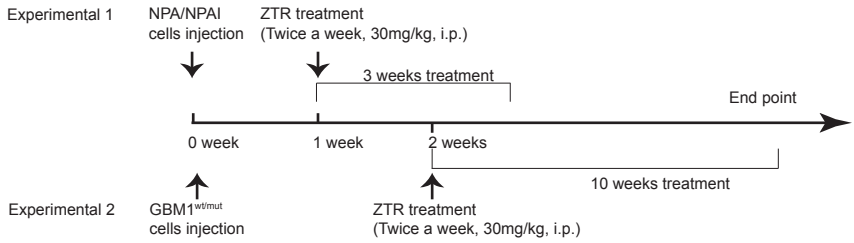

C

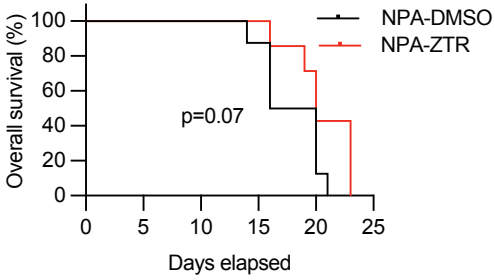

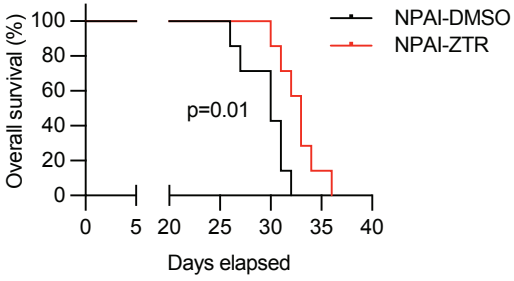

D

a

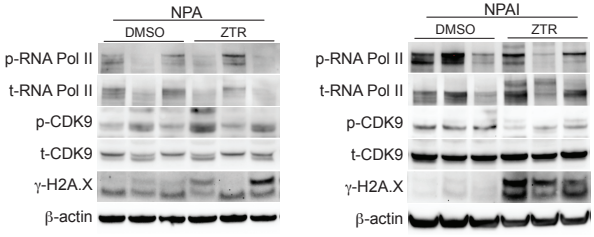

b

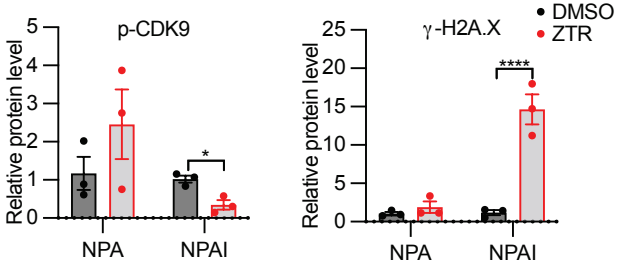

E

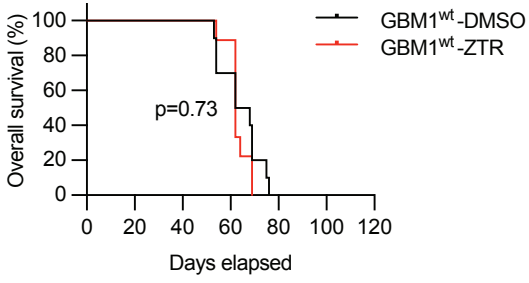

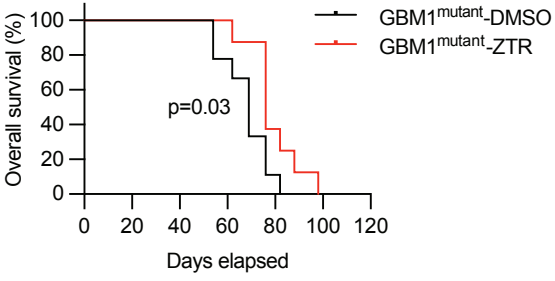
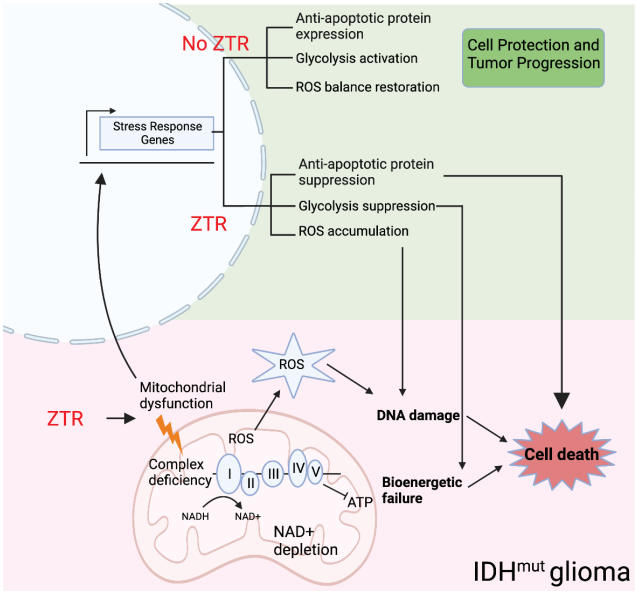
F